International Journal of Fatigue 163 (2022) 107087

Contents lists available at ScienceDirect

International Journal of Fatigue

journal homepage: www.elsevier.com/locate/ijfatigue

Influence of the rolling of contact pads on crack initiation in fretting fatigue tests

Diego Erena *, Vicente Martín, Jesús Vázquez, Carlos Navarro

Universidad de Sevilla, Escuela Técnica Superior de Ingenieros, Departamento de Ingeniería Mecánica y Fabricación, Camino de los Descubrimientos s/n, C.P. 41092, Spain

ARTICLE INFO

Keywords:
Fretting fatigue
Rolling
Fatigue crack initiation
Crack path

ABSTRACT

This work performs a detailed analysis of the cracks obtained in fretting fatigue tests with cylindrical contact in the presence of a small oscillatory rolling of the contact pad. To do so, fretting fatigue tests have been carried out. Preliminary observations indicate that the contact area is larger than the theoretical one according to Hertz's theory. This could mean that, due to the contact geometry and the stiffness of the test setup, rolling of the contact pad is occurring during tests. To reproduce this phenomenon, a 2D numerical model is developed. The results are compared with actual crack profile measurements.

1. Introduction

Fretting is a common material damage appearing in mechanical contacts under the action of time-varying loads. This material damage phenomenon is caused by small oscillatory relative surface displacements –due to the fluctuating loads– and the friction between the contacting surfaces. In many practical applications, the amplitude of the relative displacements is on the order of thousandths or hundredths of a millimetre, and a partial slip regime, in which the contact zone is divided between slip and stick zones, is usually found [1-3]. Both contact loads, normal and tangential, produce a stress field with high values and a steep gradient -especially very close to the contact edges- that varies in phase according to the relative displacements [3]. These time-varying stresses/strains can initiate small surface cracks at the hot-spot contact zones, usually located at the edges of the contact areas [2,4-6], that can grow through the zone where stresses are high enough. These relative displacements are generally produced by fluctuating global loads, or displacements, remotely applied to the elements in contact that lead to a bulk or global stress in the components [7]. If the amplitude of the global stress is high enough, the fretting initiated surface cracks can continue growing until the complete fracture of the components. There are many examples of mechanical elements suffering from fretting fatigue failure, such as bolted or riveted joints, rotor-blade dovetail connections, metal cables, or shrink-fitted couplings [8].

Testing a real component to know the fretting fatigue behaviour of a certain material, or treatment, is very unusual, so a simplified test in which geometries and contact loads lead to explicitly known stress/strain fields, is often used to replicate this phenomenon in laboratory conditions. Using this type of test, it is possible to understand the fretting crack initiation and propagation mechanisms via the analytical equations defining the stress and strain fields [9,10].

Among the wide variety of contact pairs used in fretting fatigue tests, likely one of the most used is the so called "cylindrical contact" in which a flat surface is placed in contact against a cylindrical one. The analytical stress fields in this type of contact are well described and this is one of the reasons of its common use for research purposes. A complete understanding of the fretting fatigue phenomenon is still being an important challenge due to the considerable amount of agents involved. The bibliography has a large number of studies that try to develop the best methodology to estimate the lifetime on the fretting fatigue tests and propose predicting fretting fatigue models [11-16]. There are many agents involved in the fretting phenomenon and little by little they are being studied, understood and added to fretting fatigue models to make them more robust and accurate. Two examples can be fretting wear or the residual stress relaxation in cases with surface treatments [13,17-19]. The majority of proposed life assessment models assume that the crack is perpendicular to the contact surface, which is a good approximation in terms of life prediction. However experimental measurements show that cracks initiate and propagate with a certain angle. On this study the focus is to shed light in a new agent in fretting that is not taken into account so far and could affect significantly both crack initial orientation and life prediction.

* Corresponding author.
E-mail address: deg@us.es (D. Erena).

https://doi.org/10.1016/j.ijfatigue.2022.107087
Received 19 January 2022; Received in revised form 19 May 2022; Accepted 15 June 2022
Available online 18 June 2022

One important feature in these type of tests, that is due to the compliance of the device with the tangential load, is the small rotation/rolling that can be produced between the contacting surfaces. Rolling causes that the contact zone changes during the fretting cycle; tangential load fluctuates with time and thus the contact zone as depicts Fig. 1.

It is clear that the variation in time of the contact zone location leads to a different surface contact stress distributions from that obtained using the classical Cattaneo-Mindlin approach, [20,21]. In the Author's best knowledge, there is no analytical solution for a transient tangentially loaded rolling contact, for this reason in the present work we analyse -by means of a FEM model- the effect on the crack initiation behaviour caused by the small rolling in fretting tests. The cyclic rolling was quantified indirectly via experimental measurements of the contact zone length in fretting tests [22], assuming that the difference between the theoretical and the experimental value is due to this phenomenon. Then, the inferred rolling is introduced in the FEM model, and the resulting stress/strains fields are used to predict the fretting behaviour observed in tests.

2. Experimental campaign

The contact pair studied in the current work is the usually called cylindrical contact in which a cylindrical contact pad of radius, R, is pressed against a flat surface. A scheme of the device used to conduct the test is show in Fig. 2. This device has been used for large campaigns of cylindrical and spherical fretting fatigue test during the last decades [6,5,23]. In that test setup, first of all the cylindrical contact pads are pressed against the flat surface of a dog-bone type fretting fatigue test specimen with a constant normal load, N. Then, a fully reversed cyclic axial load of amplitude, P_a, is applied directly to the specimen by means of a hydraulic actuator. The tangential load amplitude, Q, appearing as a consequence of the contact pair and the axial load P, can be adjusted to the desired value, moving the adjustable supports acting as leaf springs (see Fig. 2**a**), and thus modifying device's stiffness. Main specimen and pad parameters are shown in Fig. 2**b**.

Both contact pads and test specimens were made in aluminium alloy Al 7075-T651, which is widely used in the aircraft industry [24,25]. The chemical composition and relevant mechanical properties for this material are shown in Table 1 and Table 2.

Table 3 shows the fretting fatigue tests that are analysed in the current work with the corresponding fretting loads. In addition, the main theoretical parameters –using the plane strain Hertzian theory for elastic contacts- are also shown in the table in order to ~~ease~~ make easier the comparison of the fretting conditions among different tests. In that table, a_H is the Hertzian theoretical contact semi-width and $\Delta\sigma_{xx}$ is the analytical range of the direct/axial stress at the contact trailing edge, $x = a_H$. These two parameters are defined by the following equations [9]:

$$a_H = \sqrt{\frac{8N^*R(1-\nu^2)}{\pi E}} \tag{1}$$

$$\Delta\sigma_{xx} = \sigma + 4\mu p_0 \frac{c}{a_H}\sqrt{\left(\frac{a+e}{c}\right)^2 - 1} \tag{2}$$

Which in turn are obtained by means of $N^* = N/t$ (being t the test specimen thickness), the amplitude of the test specimen bulk stress, $\sigma = P_a/A$, the maximum surface normal pressure, p_0, the contact stick zone half-width, c, the eccentricity of the stick zone, e, and the coefficient of friction μ; this last parameter is consider equal to 0.75 [6]. The expressions for the above parameters are [9]:

$$p_0 = \frac{2N^*}{\pi a_H} \tag{3}$$

$$c = a_H\sqrt{1 - \left|\frac{Q}{\mu N}\right|} \tag{4}$$

$$e = \frac{R\sigma(1-\nu^2)}{\mu E} \tag{5}$$

Due to the fretting fatigue device's flexibility and the contact geometry, small pad rotations are observed during tests. This preliminary observation gives rise to the study developed in this work. According to the Hertźs theory the contact semi-width, a_H, depends exclusively on the normal load, material properties and pad radius, R (see **Eq. (1)**). To confirm the theory some static tests were carried out to the cylindrical contact pair applying only a normal load N. Before testing the possible contact area was covered with a layer of magnesium oxide powder (grain size of 1 μm). After testing the specimen contact area was analysed and measured in an optical microscope (see Fig. 3). As the contact zone is not perfect, the procedure described in the next section was used to estimate an average value of the contact semi-width. Noticing that the theoretical semi-width, according to **Eq. (1)** agrees very well with the experimental measurements with errors below 5%, thus validating Hertźs contact width estimation.

2.1. Fretting scar and crack measurements

This section explains the actual rotation of the pads during tests and the techniques employed to measure the fretting scars and the crack profiles of test shown in Table 3. On one hand, Fig. 4**a** depicts a scheme of the traditional contact pair studied thus far, in which the contact semi-width, a_H, keeps constant along the fretting cycle and depends exclusively on the contact pressure, besides the geometrical and material parameters. On the other hand, Fig. 4**b** depicts the actual movement of the pad while rolling is occurring. Due to the device stiffness when the tangential load is applied, the pad tends to move forward or roll to the same direction of the tangential load. Therefore, although at each instant between the extremes of the cycle, the contact semi-width continues to be a_H the scar drawn on the contact surface is larger than the theoretical one. This is due to the forward and backward movement of the pad along each cycle. Therefore, after testing, the measured scars do not represent the theoretical value according to Hertźs theory but this value displaced in both directions, left and right. Therefore, the actual semi-width of the scar, measured after testing, which should be larger than the theoretical one, will be called from now on as a_R. Besides, in Fig. 4**b** the parameter x_c represents the surface coordinate position at which crack initiates. This position is determined experimentally and will be used in subsequent sections.

To corroborate the aforementioned hypothesis, the fretting scars of test in Table 3 are measured from pictures obtained with an optical microscope and compared with theoretical values. Obviously fretting marks are not perfect and the contact area is irregular as can be seen in Fig. 5**a.** Therefore, to obtain an accurate value of the actual contact area a CAD software is used to draw the experimental contact profile and thus obtaining the actual area (see Fig. 5**a**). Dividing the true scar area by the actual scar thickness, t_s, an average value of the contact width is obtained, $2a_R$, approximating thus the contact area to a rectangle as depicts Fig. 5**b.** Before drawing the CAD profile that defines the true scar area it is important to note that at the bottom part of the scar (see Fig. 5**a**) there are several scratches that could be confused with the contact area.

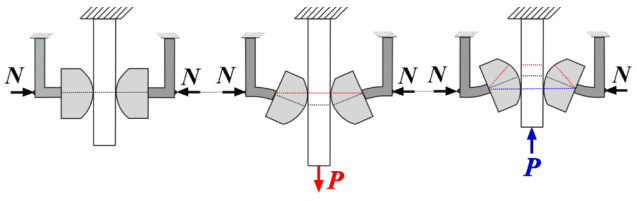

Fig. 1. Scheme of the fretting pad movement and its evolution in function of the bulk load.

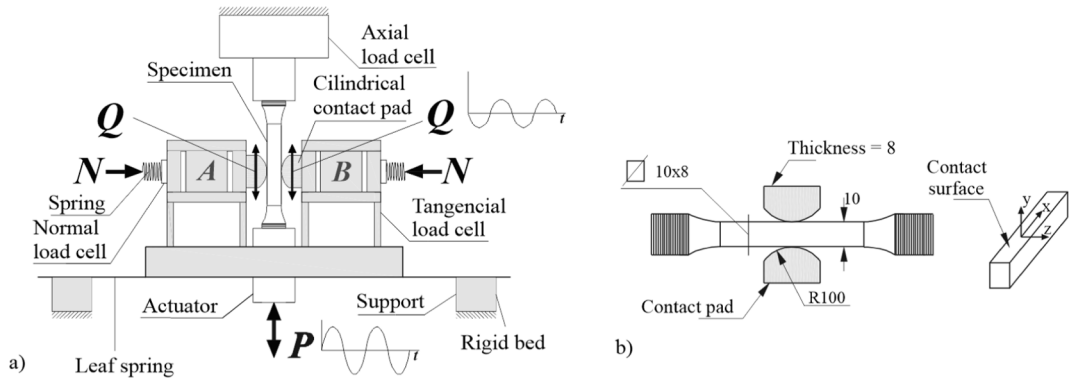

Fig. 2. a) Scheme of the fretting fatigue device used in the experimental campaign; b) main geometric characteristics –in mm- for the "dog bone" type fretting fatigue test specimens and contact pads.

Table 1
Chemical composition (% weight) for the Al 7075-T651 [18].

%	Al	Zn	Mg	Cu	Fe	Si	Mn	Cr	Ti	Others
Max	91.4	6.1	2.9	2.0	0.5	0.4	0.3	0.28	0.2	0.05
Min	87.1	5.1	2.1	1.2	–	–	–	0.18	–	–

Table 2
Main mechanical and fatigue properties for the Al 7075-T651.

Young's modulus [26]	E	71 GPa
Poisson's ratio [26]	ν	0.33
Yield strength*	σ_y	503 MPa
Tensile strength*	σ_u	572 MPa
Grain size*	d	50 μm

* Data obtained in our laboratory.

Table 3
Fretting fatigue loads and related Hertzian parameters for analysed tests.

Test	N (N)	Q (N)	σ (MPa)	a_H (mm)	p_0 (MPa)	$\Delta\sigma_{xx}$ (x = a_H)	N_f (Cycles)
1	4217	1543	110	1.30	258.6	810.7	88216–89376
2	5429	971	150	1.47	293.4	1086.3	47737–51574
3	5429	1543	150	1.47	293.4	1026.3	50268–39202

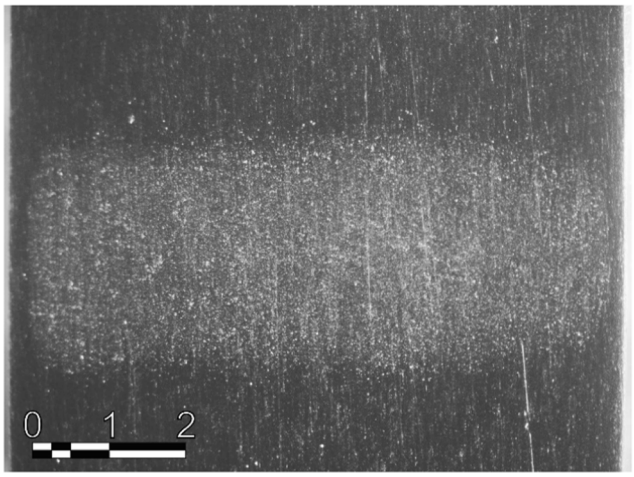

Fig. 3. Static test mark with magnesium oxide layer.

However, these scratches are produced at the last cycle of the test, that is when the specimen completely fractures, and are produced by the specimen due to the sudden failure. Notice that this measurement is done on the pad surface since the specimen surface is broken into two parts. Although the pad profile is curve, the pad radius is large enough if compared with the contact width to neglect the effect of the curvature (see Fig. 6).

Then, once the rolling semi-width, a_R, is known it is possible to obtain the crack initiation surface position, x_C, by analysing the specimen contact surface. To do so, the same procedure carried out in the last paragraph is now applied to the specimen surface. Fig. 5**c** shows a microscope photo obtained joining the broken parts, where the crack can be easily seen. The area covered from the non-damaged contact edge (leading edge) up to the crack is obtained by means of the CAD software. If the obtained area, called A_C, is divided by the true scar thickness, t_S, we obtain an average value that indicates the distance from the leading edge up to the crack. Finally, considering as reference the leading edge (top edge in Fig. 5**a** and **c**) it is possible to draw the approximated rectangles obtained for the true scar area and the new one. Both with one side superimposed, as the leading edge is the same, and thus obtaining the crack surface initiation position, x_C, considering the x-axis origin at the middle of the contact width.

The described procedure is applied to the tests and the results are shown in Table 4. The theoretical and experimental semi-widths are compared in Table 4, corroborating that the experimental fretting scars are larger than the theoretical ones.

The arc length of the new surface that comes into contact due to rolling, s, could be obtained from the difference between the experimental semi-width and the theoretical one, as shown in Table 4 and Fig. 5. Then, knowing the arc length and also the pad radius ($R = 100$ mm) the rotated angle, α, could be obtained (see Table 4). Besides, the crack initiation surface position measured, x_C, corroborates that cracks initiate slightly inside of the actual contact zone and not at the trailing edge as hertzian theory states.

The crack surfaces are also measured by means of a confocal microscope to obtain three-dimensional maps, specifically, close to the contact surface. An example is shown in Fig. 7 where an area of 0.4 mm by 0.24 mm is shown. As the obtained map is 3D it is possible to intersect some parallel planes to obtain crack profiles at different z-coordinates. These planes intersect with the 3D map obtaining thus the 2D crack profiles. These cutting planes will be around points where the cracks

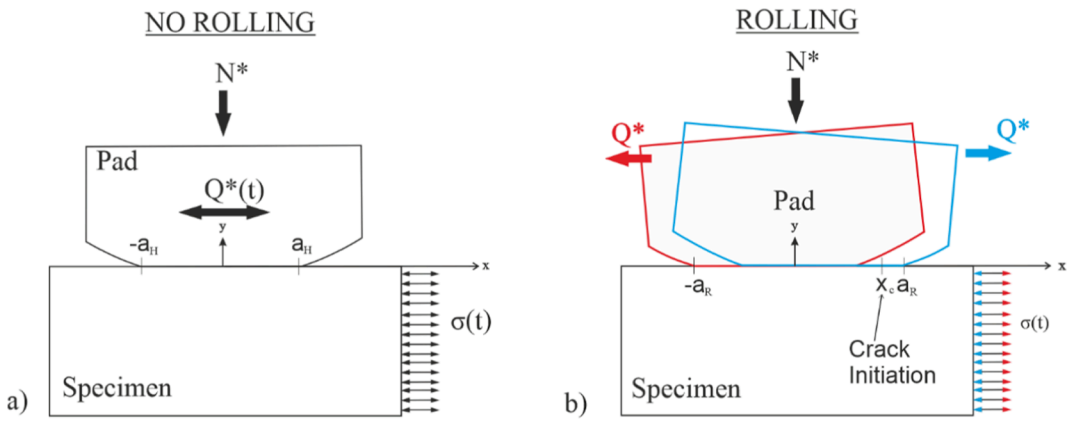

Fig. 4. (a) Scheme of the cylindrical contact without rolling; (b) Scheme of the cylindrical contact with rolling.

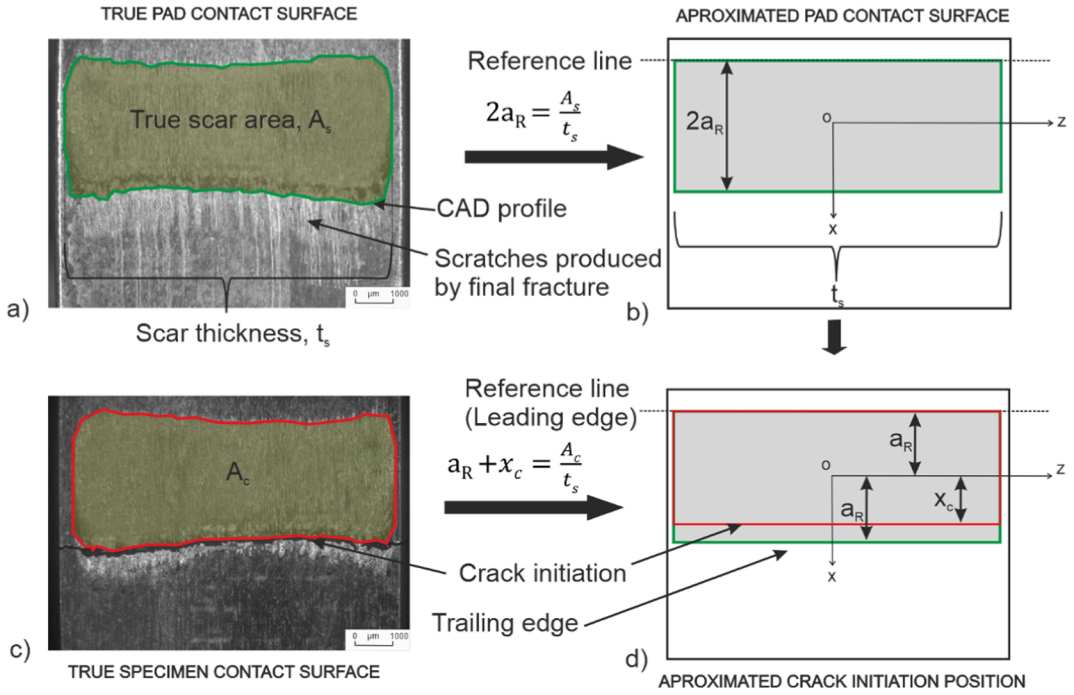

Fig. 5. Procedure to experimentally obtain the contact semi-width with rolling, a_R, and crack surface position, x_C.

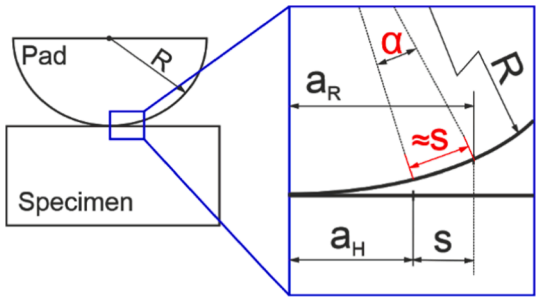

Fig. 6. Scheme of the procedure to obtain the rolling distance and angle.

possibly initiated. The obtained profiles will be shown in the results section, where comparisons with predicted paths will be also included and commented.

Table 4
Fretting fatigue rolling parameters.

Test	a_R (mm)	a_H (mm)	$s = a_R - a_H$	a_R/a_H	$\alpha = s/R$ (°)	x_c	x_c/a_R	x_c/a_H
1	1.64	1.30	0.34	1.26	0.19	1.41	0.86	1.08
2	1.74	1.47	0.27	1.18	0.15	1.54	0.89	1.05
3	1.80	1.47	0.33	1.22	0.19	1.48	0.82	1.01

3. Numerical model

The aforementioned test configuration is modelled in ANSYS® software. Taking advantage of the symmetry of the test setup, only one of the two contact pair is modelled. Boundary conditions and most significant dimensions for that model are shown in Fig. 8**a**. To reproduce the test performance, loads are applied in six steps (see Fig. 8**b**). The increments in all loading steps is very small to capture the steep contact surface distribution with the highest fidelity and confidence. The first step applies the normal load, $N^* = N/t$ ($t = 8$ mm), and it is kept constant during the remaining steps. The second step applies at the same time a

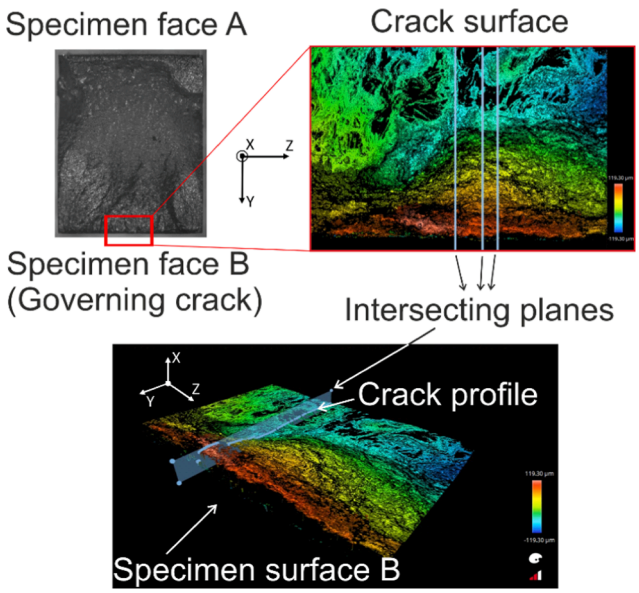

Fig. 7. Crack surface measurements using a confocal microscope.

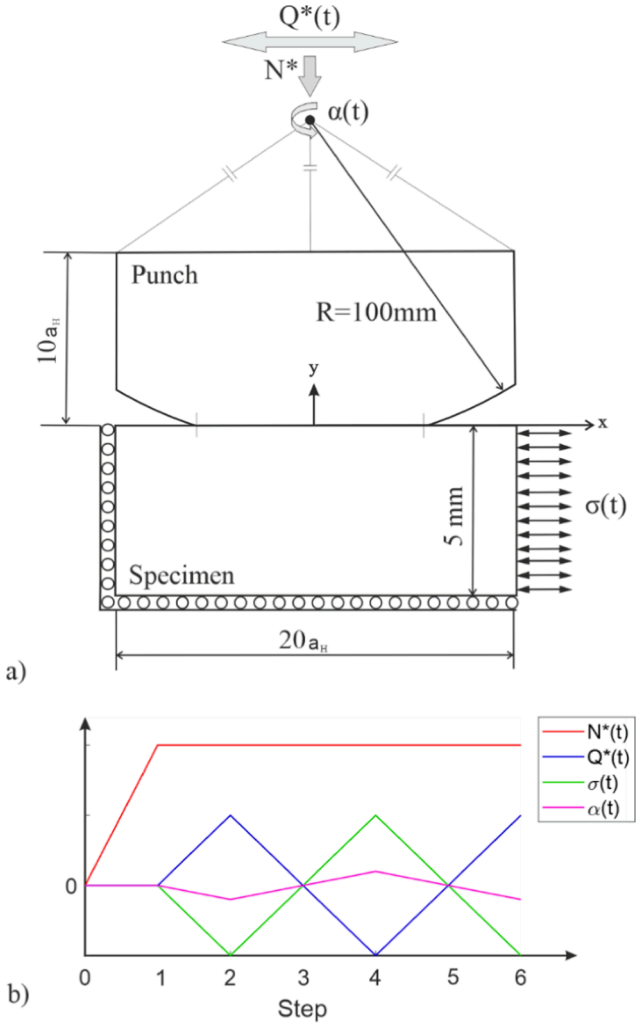

Fig. 8. (a) Scheme of the cylindrical contact pair and boundary conditions; (b) Loading steps.

tensile bulk stress, a tangential force to the left, $Q^*=Q/t$, and a counter clockwise rotation to the pad, α. The third step returns to the initial state, but maintaining the normal load. In the fourth state, loads are applied in the same manner as step 2 but in opposite directions. The step 5 returns to a state equal to step 3 and finally step 6 repeat loads from state 2. Loads Q^* and N^* and the rotating angle α, are applied to a master node, located at the geometrical centre of the pad, that transfer these loads to all nodes lying on the top of the pad (see Fig. 8**a**). The rotation of the master node is restricted in the no-rolling cases.

The element type used for modelling the components is the PLANE182, which is a 2D plane element, with 2 degrees of freedom at each node, linear formulation, and 2 possible element shapes: triangular and quadrilateral. Due to the pads and test specimens' dimensions, it is suitable to use a plane strain formulation [27]. Due to the strong gradients appearing on the contact surface, the mesh size was carefully studied in order to faithfully capture them. After a convergence analysis we decided that an element size of 5 μm, for the elements surrounding the contact zone, was the perfect balance between accuracy and computational time. The rest of the model is meshed with triangular elements as can be seen in Fig. 9. Elements CONTA171 and TARGE169 are used to model the contact pair. The contact formulation used is the augmented Lagrange method because of its good behaviour when friction is contemplated.

4. Results

4.1. Contact surface results

Tests from Table 2 are reproduced with the numerical model. Step 4 and 6 are used to analyse a representative cycle of the fretting fatigue test. The contact surface stresses along the fretting cycle are depicted in Fig. 10 for each test. The first row of graphs shows the contact pressure distribution, the second row the shear stress, the third row the axial stress and the last one the range of axial stress. The contact pressure distribution shows the displacement of the contact zone when rolling is considered, to the right when the load Q is positive and to the left when load Q is negative. In the case without rolling, the directions of the tangential load do not influence the contact surface, as it only depends on the normal load, N. It is noteworthy how different are the shear stress distributions from the classical Cattaneo ones when rolling is considered. As a consequence of the above, the axial stresses on the contact surface differ substantially from those cases in which there is no rolling. It is remarkable how the maximum and minimum values are displaced from the theoretical edge of the contact zone. In order to better appreciate the evolution along the fretting cycle of the axial and shear stresses at the contact surface, Fig. 11 has been included. It should be noted that the extreme values of the axial stress are found when the tangential load, Q, is maximum and minimum. Although the fretting phenomena is strongly multiaxial, specially below the near contact surface material, the study of the $\Delta\sigma_{xx}$ surface stress is a good and easy approximation to the surface crack initiation process. The $\Delta\sigma_{xx}$ graphs show two plotted lines; the black is the no-rolling case in which it can be seen that the hot

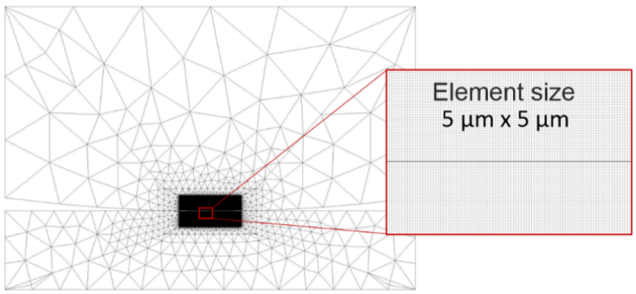

Fig. 9. FEM mesh and contact zone detail.

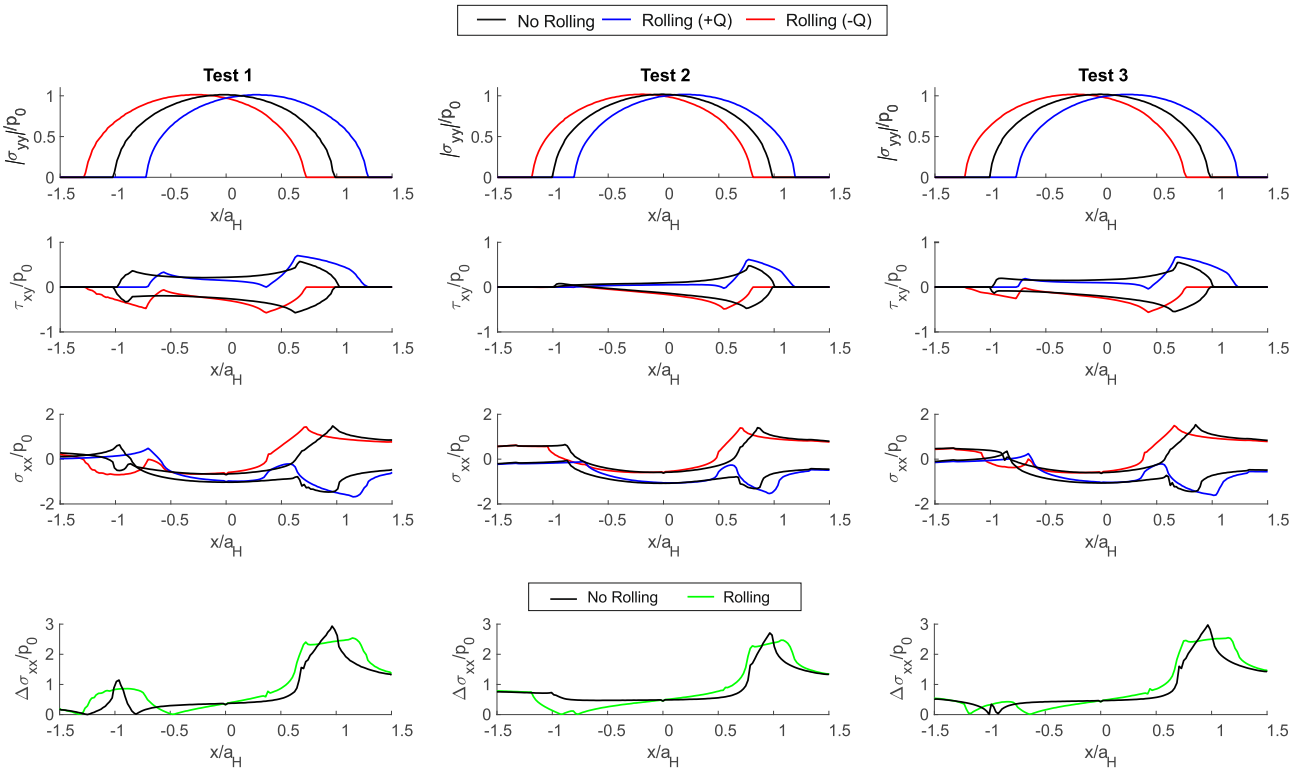

Fig. 10. Contact surface FEM results.

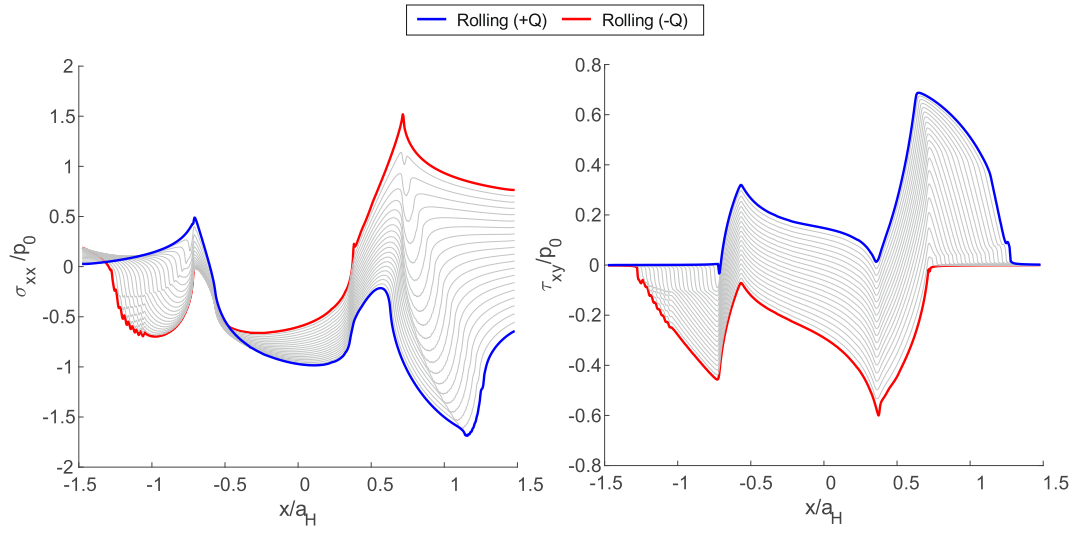

Fig. 11. Contact surface axial stress evolution for Test 1.

spot is at the contact trailing edge, i.e. as the theory states. The green line represents the configuration with rolling, and in this case it cannot be said that there is a clear point of maximum values for the axial stress range, instead there is a zone (some kind of plateau) of high stress levels in which the values are almost constant.

These preliminary numerical results are in very good agreement with the crack initiation surface coordinate position measured, x_C. Although simulations show that there is not a clear point for crack initiation, the maximum values of $\Delta\sigma_{xx}$ are found in a range approximately between $0.8a_H$ and $1.2a_H$. These values are in line with experimental cracks which were observed inside this range (between 1.01 a_H and 1.08 a_H) and not at the contact edge as Hertz theory states. Moreover, as the trailing edge is not fixed in the case of rolling, it moves as the loads are applied, the maximum axial stress range is lower than the case without rolling. These preliminary results suggest that rolling should be taken into account when tests are carried out in laboratory conditions for some fretting machines that allow some pad rotations.

In previous authors works the SWT parameter has demonstrated its potential to estimate both, the contact surface hot-spot and the initiation and propagation crack path, for non-rolling cases [28]. With the aim of analysing the hot-spot point at the contact surface for the rolling case, the hot spot point is studied by means of the SWT parameter. The traditional SWT parameter for uniaxial loading is shown in **Eq.** (6). However due to the multiaxial characteristics of the loading states in fretting, **Eq.** (7) is more adequate, which is an extension of the original one for the case of non-proportional loading states and proposed by

Marquis & Socie [29].

$$SWT = \sigma_{max}\frac{\Delta\varepsilon}{2} \tag{6}$$

$$SWT = \left(\sigma_n{}^{max}\frac{\Delta\varepsilon}{2}\right)_{max} \tag{7}$$

In the above equations, σ and $\Delta\varepsilon$ are the stress and the range of the strain normal to the material plane and over the loading cycle. The difference between both formulations of the parameter is the definition of the critical plane, in **Eq. (6)** the critical plane is defined by that producing the maximum strain range and then is scaled by the normal stress at the same plane. In the case of **Eq. (7)** the critical plane is defined by that producing the maximum value of the product. As it is well known, the stress/strain field in fretting are non-proportional. However, at the contact surface and close to the trailing edge the stress/strain non-proportionality is negligible, this could be corroborated analysing Fig. 11. For this reason, as the results are similar, the hot spot point at the contact surface will be obtained only with **Eq. (7)**. Later, in the crack orientation section both formulations will be compared, since in this analysis the stress/strain fields below the contact surface are important and at these depths the non-proportionality is not negligible.

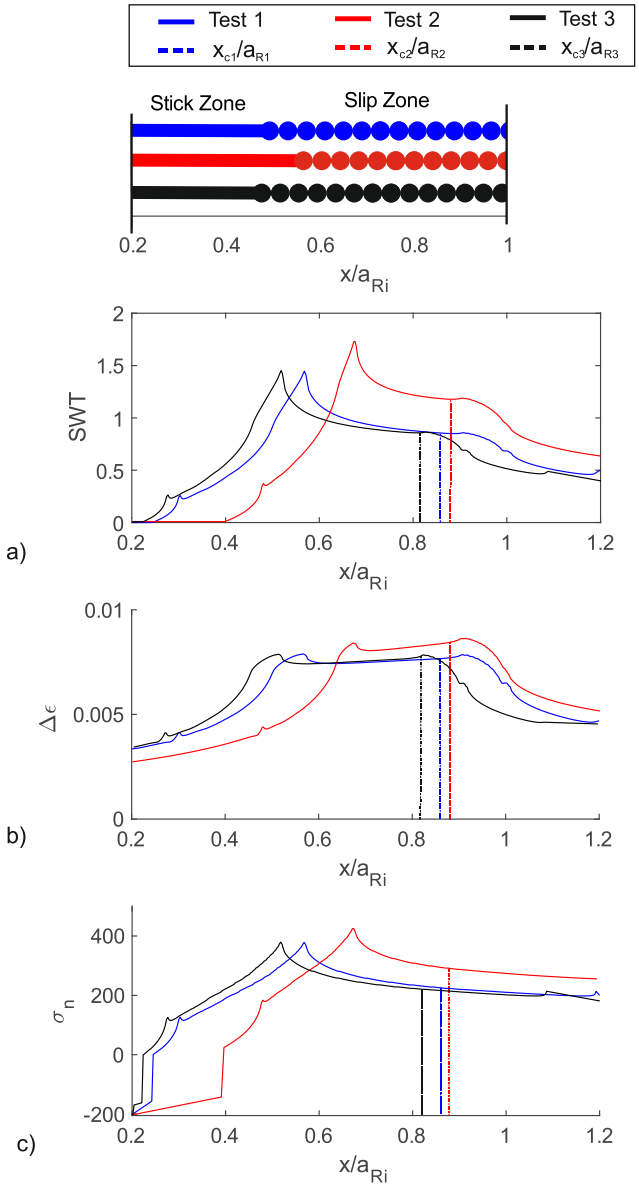

Fig. 12. Surface distribution: (a) SWT parameter; (b) Range of axial strain; (c) Axial maximum stress.

Fig. 12**a** depicts the SWT values at the contact surface for the rolling cases applying **Eq. (7)**. The critical plane orientation is not represented as it is not relevant for the estimation of the surface hot-spot position. The cases without rolling are not included to not blurring the figure, in these cases the maximum value of the parameter is always obtained at the trailing edge. The curves of Fig. 12**a** show a maximum of the parameter in the range x/a_{Ri} = [0.5–0.7], values that are far from the experimental crack initiation position, x_c (included in the figure with vertical dotted lines). Therefore, the SWT is not able to assess the crack initiation point when rolling is taken into account. To look for an explanation, the parameters used to calculate the SWT are represented individually. These parameters are the normal strain, $\Delta\varepsilon$, and the maximum normal stress to the critical plane (the plane maximising the product), depicted in Fig. 12**b** and Fig. 12**c** respectively. Analysing Fig. 12**b**, it is difficult to define a maximum value but a zone of maximum values. The same could not be said with the normal stress of Fig. 12**c**, which shows a maximum value at the same points of Fig. 12**a**. Therefore, this is the reason why the SWT parameter is not able to detect the actual hot-spot. Up to now, the SWT parameter has been applied to numerical results obtained from simulations without rolling, where all contact points were always at the same position. In the non-rolling cases the maximum of both stress and strain is always at the contact trailing edge and therefore also the SWT parameter. In the no-rolling cases, the contact edge is always at the same position. However, with rolling the trailing edge is at a different position along the cycle due to the movement as rigid solid of the pad (see Fig. 4**b**). This is the reason why the strain range does not have a clear peak, but a kind of plateau. Then this strain range is scaled by the maximum normal stress that is found when the tangential load is minimum, -*Q*. This causes an erroneous maximum value to appear at the same position where the normal stress is at its maximum. These numerical and experimental results suggest that in the case of rolling, the strain range may be a better indication of the most unfavourable point of the contact surface, which in reality is more a zone prone to crack initiation than a point.

4.2. *Crack initiation prediction*

In this section the crack initiation path is assessed and compared with actual measurements from the confocal microscope. Fig. 13 shows a schematic representation of the method proposed based on the SWT parameter with some modifications. At first, it is necessary to define a point at the surface where potentially a crack could nucleate which will be called hot-spot, the most common way is to consider that point at the contact edge or at the point where some multiaxial fatigue parameter is maximum. This critical point is considered to be the origin of different material planes distributed homogeneously between$\theta_i = 90°$ and$\theta_i = -90°$ for a fixed radius r^*, defining the size of the influence area (see Fig. 13). The orientation, θ_i represents all possible directions of the

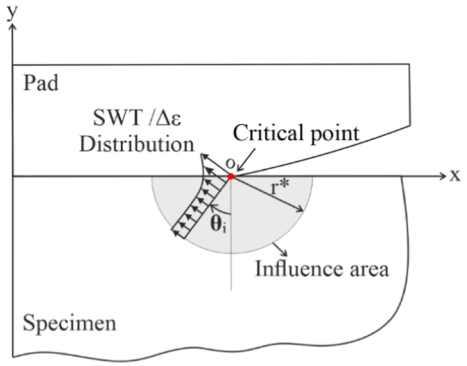

Fig. 13. Crack initiation criteria.

nucleated crack. Now, the SWT parameter is calculated along each of these lines (defined by θ_i), but with the novelty that, the orientation of the material plane considered to evaluate the parameter is not the critical one, i.e., according to **Eq. (6) and Eq. (7)**, but the one that coincides with the orientation imposed by θ_i. For example, for the 0° plane (vertical) the stresses and strains used to obtain the SWT parameter are σ_{xx} and ε_{xx} (perpendicular to the material line/plane), which potentially could produce a crack in vertical direction. With this procedure a SWT distribution (Fig. 13) is obtained along each material line/plane. Next, the mean value of the SWT distribution along each line is calculated ($\overline{SWT}$). Based on the results of the former section in which the range of axial strain produces better results than the SWT in terms of crack initiation prediction, the explained procedure is also applied for the range of normal strain.

For the no-rolling cases the critical point on the contact surface is considered at the trailing edge $x/a_H = 1$ as theory states and numerical model confirms. For the rolling cases the critical point is considered at the predicted crack initiation position (see Fig. 12). For the SWT method, the hot-spot points are those maximum values observed in Fig. 12**a** (Independently of the use of **Eq. (6)** or **Eq. (7)**). In the case of the proposed $\Delta\varepsilon_{max}$ method, there is not a clear hot-spot, for this reason two points are evaluated. These points are the extremes of the plateau (the two local maximums) of Fig. 12**b**. Note that these values have been chosen as a representation of the zone of maximum values. However, as said before, all points in this kind of plateau are candidates for crack initiation as the difference between them are minimum. The radius of the influence area, r^*, considered in the current work is 50 μm, value in accordance with the grain size of the material. Although crack initiation prediction procedure is nearly independent of this length as was observed in former works [30,31].

Some results obtained applying the described procedure are shown in Fig. 14 as a function of the θ orientation. The specific orientation where the curves achieve their maximum are depicted in Table 5 for all possible combination.

Finally, the real crack profiles measured via confocal microscope are represented in conjunction with the values of Table 5. Fig. 15**a** depicts the samples measured and the mean value obtained for each group of samples. It can be seen the wide variety of crack surface profiles for the same specimen. In Test 1 this variety is more marked than the profiles of Test 2 and 3 which follow approximately the same orientation. Fig. 15**b** shows the mean profiles and the orientations predicted, see Table 5. It should be noted that in Fig. 15 we have plotted the initiation from the same point for all curves to be able to easily compare the slopes, however the exact position of initiation of the crack on the contact surface is indicated in Table 6 for the rolling cases (non-rolling cases are evaluated at the theoretical contact edge). Analysing Table 6 it is clear that the predicted hot-spot position obtained applying the SWT parameter is not precise. In the case of the $\Delta\varepsilon_{max}$ method, as the critical zone is a range, the experimental crack position measured lies inside this range which is in more agreement with reality, as cracks are expected to initiate at several points and not at an exact position.

Table 5
Crack initial predicted orientations.

Test	No Rolling			Rolling		
	SWT_6 (**Eq. (6)**)	SWT_7 (**Eq. (7)**)	$\Delta\varepsilon_{max}$	SWT_6 (**Eq. (6)**)	SWT_7 (**Eq. (7)**)	$\Delta\varepsilon_{max}$
1	4°	3°	4°	24°	14°	24°–10°
2	3°	2°	3°	22°	13°	22°–10°
3	3°	2°	3°	30°	20°	30°–14°

Regarding the crack slope, first of all, it is clear that, independently of the prediction method used, the cases without rolling predict cracks almost perpendicular to the surface which is not in agreement with experimental results and thus corroborating the importance of rolling. The slopes predicted with both SWT formulations throw coherent results. Nevertheless, as the hot spot is not well predicted the results are not consistent. Finally, the results obtained with the $\Delta\varepsilon_{max}$ method, although it does not yield a unique and concrete value, are reasonable and in good agreement with experimental results in all senses, hot spot region prediction and initial crack slope.

5. Conclusions

The first conclusion is that the fretting fatigue bridges can produce an effect of rolling on the contact pads which increases the contact zones and this results in different contact stress and strain fields. It has been observed through the experimental measurements that the cracks initiations do not appear at the contact trailing edge but within the contact

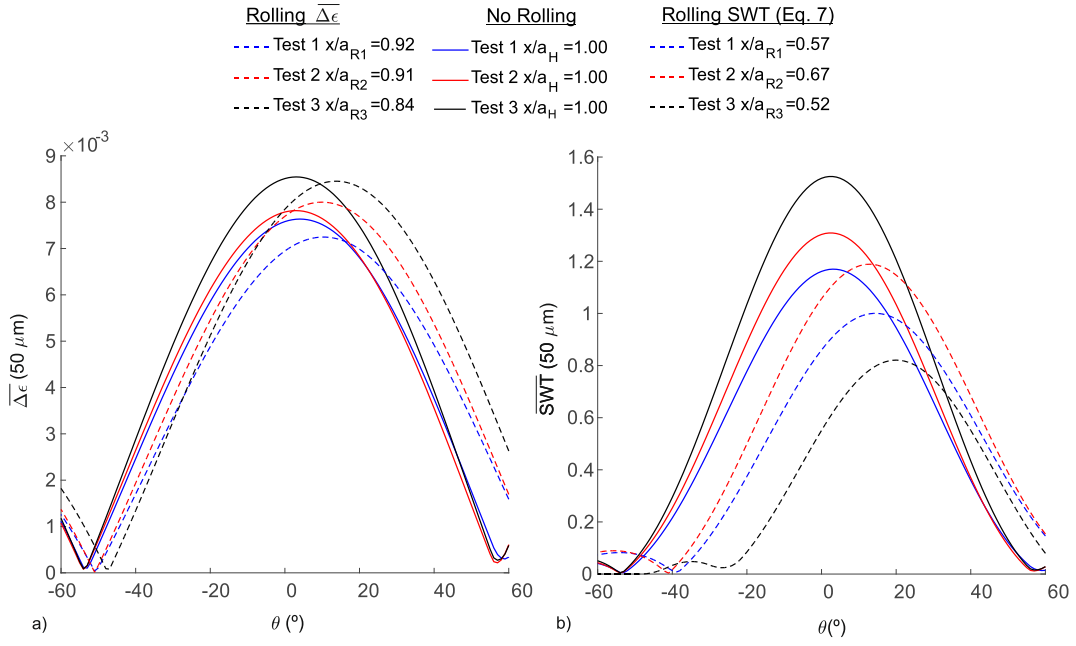

Fig. 14. Average parameter distribution in function of the initial orientation: (a) max($\Delta\varepsilon_{xx}$) method, (b) SWT method.

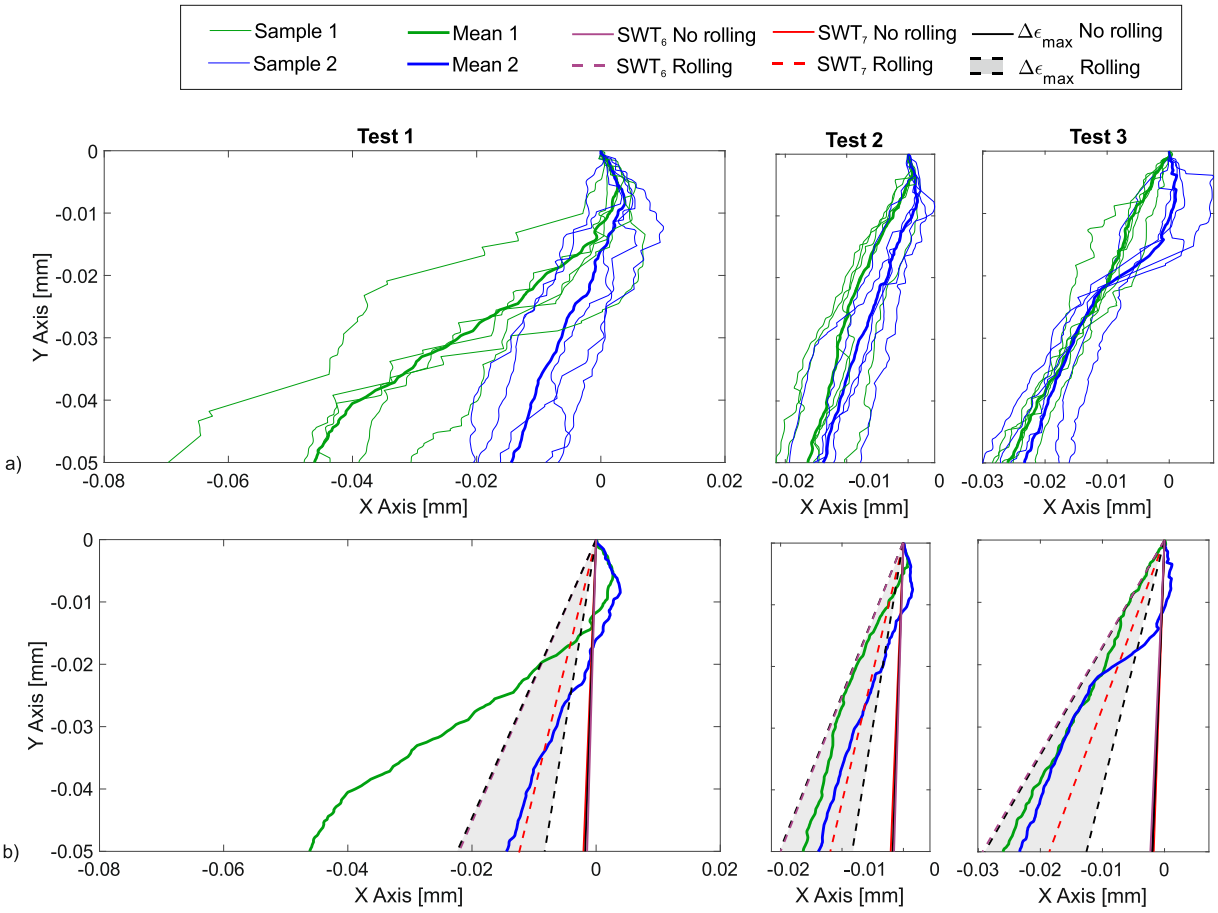

Fig. 15. (a) Actual confocal crack profiles and mean profiles, (b) Mean profile and crack predictions of Table 5.

Table 6
Crack initial predicted position.

Test		SWT_6 (**Eq. (6)**)	SWT_7 (**Eq. (7)**)	$\Delta\varepsilon_{max}$	Exp.
1	x_c/a_{R1}	0.57		0.57–0.91	0.86
2	x_c/a_{R2}	0.68		0.68–0.91	0.89
3	x_c/a_{R3}	0.52		0.52–0.84	0.82

zone, in special at the slip zone, and this is verified by the criteria applied in this work. The SWT multiaxial fatigue parameter has been studied to predict the surface hot-spot by means of two formulations, the traditional one and the adaptation to non-proportional loading states. Independently of the formulation, good results are obtained for the simulated no rolling cases but not for the rolling ones if compared with experimental measurements. Due to this observation, the range of the normal strain has been used to analyse the hot-spot for the rolling cases obtaining results more in accordance with the experimental ones.

Finally, the crack initiation angle has been calculated by means of both SWT and a strain range based method. The angles have been compared with the specimen crack profiles measurements. By this comparison, it is possible to see that, if rolling is considered, better crack initiation angles are predicted if compared with a non-rolling case independently of the method used. However, if the maximum strain range method is considered for the no rolling cases better crack initial orientations are obtained if compared with the SWT method. Corroborating thus the importance of the rolling effect in the fretting fatigue phenomenon.

Declaration of Competing Interest

The authors declare that they have no known competing financial interests or personal relationships that could have appeared to influence the work reported in this paper.

References

[1] Nishioka K, Hirakawa K. Fundamental investigation on fretting fatigue – Part 5. The effect of relative slip amplitude. Bull JSME 1969;12:692–7.
[2] Waterhouse R. Fretting fatigue. U.K: Applied Science Publishers; 1981.
[3] Mechanics of Fretting Fatique, D.A. Hills, D. Nowell, 1994, Springer, Dordrecht, https://doi.org/10.1007/978-94-015-8281-0.
[4] Nishioka K, Hirakawa K. Fundamental Investigations of Fretting Fatigue : Part 2, Fretting Fatigue Testing Machine and Some Test Results. Trans Japan Soc Mech Eng 1968;34:1183–9. https://doi.org/10.1299/kikai1938.34.1183.
[5] Vázquez J, Navarro C, Domínguez J. Experimental results in fretting fatigue with shot and laser peened Al 7075–T651 specimens. Int J Fatigue 2012;40:143–53. https://doi.org/10.1016/j.ijfatigue.2011.12.014.
[6] Martín V, Vázquez J, Navarro C, Domínguez J. Fretting-fatigue analysis of shot-peened Al 7075–T651 test specimens. Metals (Basel) 2019;9(5):586. https://doi.org/10.3390/met9050586.
[7] Nishioka K, Hirakawa K. Fundamental Investigations of Fretting Fatigue : Part 4, The Effect of Mean Stress. Bull JSME 1969;12(51):408–14. https://doi.org/10.1299/jsme1958.12.408.
[8] Jimenez-Peña C, Talemi RH, Rossi B, Debruyne D. Investigations on the fretting fatigue failure mechanism of bolted joints in high strength steel subjected to different levels of pre-tension. Tribol Int 2017;108:128–40. https://doi.org/10.1016/j.triboint.2016.11.014.
[9] Vázquez J, Navarro C, Domínguez J. A new method for obtaining the stress field in plane contacts. Int J Solids Struct 2012;49(26):3659–65. https://doi.org/10.1016/j.ijsolstr.2012.07.021.
[10] Vázquez J, Navarro C, Domínguez J. Explicit equations for sub-surface stress field in plane contacts. Int J Mech Sci 2013;67:53–8. https://doi.org/10.1016/j.ijmecsci.2012.12.006.

[11] Navarro C, Vázquez J, Domínguez J. Nucleation and early crack path in fretting fatigue. Int J Fatigue 2017;100:602–10. https://doi.org/10.1016/j.ijfatigue.2016.12.028.
[12] Carpinteri A, Vantadori S, Zanichelli A. Lifetime estimation of mechanical assemblies under constant amplitude fretting fatigue loading. Fatigue Fract Eng Mater Struct 2019;42(9):1927–36.
[13] Vantadori S, Vázquez J, Zanichelli A. Fretting fatigue and shot peening: a multiaxial fatigue criterion including residual stress relaxation. Tribol Int 2020;151:106537. https://doi.org/10.1016/j.triboint.2020.106537.
[14] Vantadori S, Zanichelli A, Araújo JA. Fretting fatigue of 7050–T7451 Al alloy: the influence of bulk mean stress. Int J Fatigue 2020;140:105816. https://doi.org/10.1016/j.ijfatigue.2020.105816.
[15] Rangel D, Erena D, Vázquez J, Araújo JA. Prediction Of Initiation And Total Life In Fretting Fatigue Considering Kinked Cracks. Theor Appl Fract Mech 2022;119:103345. https://doi.org/10.1016/j.tafmec.2022.103345.
[16] Wang C, Li C, Ling Y, Abdel Wahab M. Magd Abdel Wahab, Investigation on fretting fatigue crack initiation in heterogenous materials using a hybrid of multiscale homogenization and direct numerical simulation. Tribol Int 2022;169:107470. https://doi.org/10.1016/j.triboint.2022.107470.
[17] Pinto AL, Cardoso RA, Talemi R, Araújo JA. Early crack orientation prediction methods under fretting fatigue loading including wear effects. Int J Fatigue 2022;161:106893. https://doi.org/10.1016/j.ijfatigue.2022.106893.
[18] Pinto AL, Araújo JA, Talemi R. Effects of fretting wear process on fatigue crack propagation and life assessment. Tribol Int 2021;156:106787. https://doi.org/10.1016/j.triboint.2020.106787.
[19] Baydoun S, Fouvry S, Descartes S. Modeling contact size effect on fretting wear: a combined contact oxygenation - third body approach. Wear, Volumes 2022;488-489:204168. https://doi.org/10.1016/j.wear.2021.204168.
[20] Cattaneo, C. Sul contatto di due corpi elastici: distribuzione locale degli sforzi. Rendiconti dell'Accademia, Nazionale dei Lincei 1938;27: 342-348, 434-436, 474-478.
[21] Mindlin RD. Compliance of Elastic Bodies in Contact. J Appl Mech 1949;16:259–68. https://doi.org/10.1115/1.4009973.
[22] Martín V, Vázquez J, Navarro C, Domínguez J. Effect of shot peening residual stresses and surface roughness on fretting fatigue strength of Al 7075–T651. Tribol Int 2020;142:106004. https://doi.org/10.1016/j.triboint.2019.106004.
[23] Navarro C, García M, Domínguez J. Fretting fatigue in a spherical contact. J Strain Anal Eng Des 2002;37(6):469–78.
[24] Merati A, Eastaugh G. Determination of fatigue related discontinuity state of 7000 series of aerospace aluminum alloys. Eng Fail Anal 2007;14(4):673–85.
[25] Czerwinski F. Controlling the ignition and flammability of magnesium for aerospace applications. Corros Sci 2014;86:1–16.
[26] Alloy 7075 Plate and Sheet: Alcoa Mill Products: SPD-10-037; 2001.
[27] Vázquez J, Navarro C, Domínguez J. Two dimensional versus three dimensional modelling in fretting fatigue life prediction. J Strain Anal Eng Des 2016;51(2):109–17.
[28] Erena D, Vázquez J, Navarro C, Domínguez J. A Fretting Fatigue Model Based On Self-Steered Cracks. Theor Appl Fract Mech 2021;103144.
[29] Socie DF, Morrow J, Chen W-C. A procedure for estimating the total fatigue life of notched and cracked members. Eng Fract Mech 1979;11(4):851–9.
[30] Erena D, Vázquez J, Navarro C, Domínguez J. Voids as stress relievers and a palliative in fretting. Fatigue Fract Eng Mater Struct 2018;41(12):2475–84.
[31] Erena D, Vázquez J, Navarro C, Domínguez J. Numerical analysis of toroidal voids as stress relievers in shrink-fitted shafts. Tribol Int 2020;143:105996. https://doi.org/10.1016/j.triboint.2019.105996.